



CrossMark
click for updates

Cite this: DOI: 10.1039/c4ce02290d

Solid-state identity of 2-hydroxynicotinic acid and its polymorphism†

Sihui Long,^{‡a} Panpan Zhou,^{‡b} Kathryn L. Theiss,^c Maxime A. Siegler^d and Tonglei Li^{*e}

2-Hydroxynicotinic acid (2-HNA), a derivative of nicotinic acid, was found to exist in four polymorphs. In the solid state, 2-HNA is actually present as its tautomer, 2-oxo-1,2-dihydro-3-pyridinecarboxylic acid (2-ODHPCA). The polymorphism stems from distinctive packing arrangements of the molecules, and the formation of the distinct polymorphs can be affected by using various acidic additives. The thermal behaviors of the four polymorphs indicate that form I is the most stable at elevated temperature, form II converts into form I during heating, and forms III and IV transform into form II when heated. Theoretical studies showed that 2-ODHPCA is more energetically favored than 2-HNA. Condensed Fukui functions and the dual descriptor were used jointly to examine the local preference of hydrogen bonding in the crystal. Lattice energy calculations were conducted to further evaluate energetic properties of the system.

Received 19th November 2014,
Accepted 5th January 2015

DOI: 10.1039/c4ce02290d

www.rsc.org/crystengcomm

1. Introduction

2-Hydroxynicotinic acid (2-HNA), a derivative of nicotinic acid is of great importance in many areas. For example, it can be used for treating atherosclerosis and hypoglycemia,¹ for synthesizing pharmaceuticals and agrochemicals,^{2,3} as well as for coordinating to metal ions.^{4,5} Structurally, 2-HNA can be viewed as an enol form, while it can also exist as a ketonic form. Because the hydrogen on the OH group is labile and in the α position to the pyridine N atom, it readily migrates to N, forming 2-oxo-1,2-dihydro-3-pyridinecarboxylic acid (2-ODHPCA), the tautomer of 2-HNA (Scheme 1). Such a phenomenon makes 2-HNA versatile in many chemical processes.

The enol-ketonic tautomerization in solution phase has attracted great interest.^{6,7} Dogra investigated the spectroscopic characteristics of 2-HNA in different solvents and under various pH conditions with a variety of spectroscopic methods and quantum chemistry calculations.⁸ The studies suggest that neutral 2-HNA is negligible in various types of solvents without pH adjustment due to the tautomerization. In the solid state, the keto form may also be favored because 2-ODHPCA could be more stable than 2-HNA due to the

formation of intramolecular hydrogen bonding between the carboxyl OH and carbonyl C=O. Yet no crystal structure was reported until we obtained the first one (designated form I) when we conducted a chemical synthesis using 2-chloronicotinic acid (2-CNA) as a reactant in water.⁹ The hydrolysis of 2-CNA led to 2-HNA, and the real identity of 2-HNA in the crystal was revealed to be its tautomer 2-ODHPCA. Note that this molecule has multiple functional groups which can participate in various hydrogen bonds, and moreover, the pH value would also affect the distribution of different forms in solution. To explore possible 2-HNA in the solid state and new forms of 2-ODHPCA, polymorph screening of the compound was conducted. Encouragingly, three new crystals were obtained, but they were all forms (forms II, III, and IV) of 2-ODHPCA, making 2-ODHPCA a new system with at least four polymorphs, a rarity especially for a small and rigid molecule. Noticeably, form II was also attained by Santos and coworkers in the study of the complexation between cobalt(II) and 2-HNA.¹⁰ Herein, the structural features of four polymorphs, their thermal properties, and the pH effect on the polymorph control were reported in detail. In addition, to shed light onto the formation mechanisms of four different polymorphs, theoretical calculations were performed.

^a School of Chemical Engineering and Pharmacy, Wuhan Institute of Technology, Wuhan, Hubei, China

^b Department of Chemistry, Lanzhou University, Lanzhou, Gansu, China

^c Department of Pharmaceutical Sciences, College of Pharmacy, University of Kentucky, Lexington, Kentucky, USA

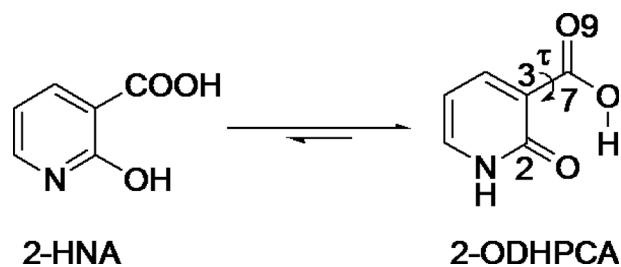
^d Department of Chemistry, Johns Hopkins University, Baltimore, Maryland, USA

^e Department of Industrial and Physical Pharmacy, Purdue University, 575 Stadium Mall Drive, West Lafayette, Indiana 47907, USA.

E-mail: tonglei@purdue.edu; Tel: +1 765 494 1451

† CCDC 1035032, 1035033, 1035034, 1035035. For crystallographic data in CIF or other electronic format see DOI: 10.1039/c4ce02290d

‡ S.L. and P.Z. contributed equally.



Scheme 1

2. Experimental section

2.1 Materials

All solvents and reagents were purchased from commercial sources and used as received. 2-HNA was firstly produced as a by-product in the laboratory,⁹ and a commercially available product (purchased from Alfa Aesar) was also used later in the study of polymorph screening.

2.2 Crystal growth, structure determinations and characterizations

2-HNA was initially obtained during an attempt to synthesize 2-(2,4-dichloro-6-methylphenylamino)nicotinic acid by reacting 2-chloronicotinic acid and 2,4-dichloro-6-methylaniline (DCMA) in the presence of pyridine and *p*-toluenesulfonic acid (*p*-TsOH) in water, apparently through hydrolysis of 2-CNA.⁹ The crude product from the reaction mixture was dissolved in ethyl acetate, water and methanol, respectively. The solutions were set for slow evaporation. Of the commercially available 2-HNA, both slow evaporation and slow cooling were applied for crystal growth. For the slow evaporation, 2-HNA was dissolved in different solvents (aqueous and organic) forming saturated solutions with or without the intentional addition of additives at ambient temperature (Tables 1 and 2). The solutions were set for slow evaporation until single crystals were harvested. For example, 50 mg of 2-HNA was added to 20 mL HPLC grade methanol. The mixture was stirred overnight and the remaining solid was removed by pipette filtration. The vial with clear solution was covered with perforated parafilm. Slow evaporation led to single crystals in about a week. For slow cooling, a supersaturated solution of 2-HNA was prepared in an Erlenmeyer flask with heating to the temperature right below the boiling point of a given solvent on a hot plate. The solution was gradually cooled to room temperature on the hot plate with power off. Crystals were recovered by filtration. All crystallization experiments were conducted in

Table 1 Crystal growth of 2-HNA in different solvents without additives

Solvent	Growth condition	Polymorph
Methanol	Slow evaporation or slow cooling	II
Ethanol	Slow evaporation or slow cooling	II
Water	Slow evaporation or slow cooling	II
Iso-propanol	Slow evaporation or slow cooling	II
Acetone	Slow evaporation or slow cooling	II
Dimethyl sulfoxide	Slow evaporation or slow cooling	II
Ethyl acetate	Slow evaporation or slow cooling	II
<i>N,N</i> -Dimethylformamide	Slow evaporation or slow cooling	II
Acetic acid	Slow evaporation or slow cooling	II

Table 2 Crystal growth of 2-HNA in different solvents with additives

Solvent	Additive ^a	Growth condition	Polymorph
Methanol	2-CNA	Slow evaporation	II
Methanol	DCMA	Slow evaporation	II
Methanol	2-CNA and <i>p</i> -TsOH	Slow evaporation	I
Methanol	DCMA and <i>p</i> -TsOH	Slow evaporation	I
Methanol	<i>p</i> -TsOH	Slow evaporation	I, II
Methanol	<i>p</i> -TsOH	Slow cooling	I, II, IV
Methanol	HCl	Slow evaporation	I
Ethanol	2-CNA	Slow evaporation	II
Ethanol	DCMA	Slow evaporation	II
Ethanol	<i>p</i> -TsOH	Slow evaporation	I, II, IV
Ethanol	<i>p</i> -TsOH	Slow cooling	I, II, IV
Ethanol	HCl	Slow evaporation	I
Acetone	<i>p</i> -TsOH	Slow evaporation	I, II
Ethyl acetate	<i>p</i> -TsOH	Slow evaporation	I
Water	<i>p</i> -TsOH	Slow cooling	I, II, III, IV

^a 2-CNA = 2-chloronicotinic acid, DCMA = 2,4-dichloro-6-methylaniline, *p*-TsOH = *para*-toluenesulfonic acid, and HCl = hydrochloric acid.

an unmodified atmosphere. Each experiment was repeated multiple times. Specifically, the following protocols were utilized to generate all four forms. For form I, dissolve 525 mg of 2-HNA together with 15 mg *p*-TsOH in 25 mL methanol during heating, remove the excess 2-HNA by filtration, cool down the solution to room temperature gradually and recover the crystals by filtration; for form II, dissolve 500 mg 2-HNA in 25 mL methanol by heating, remove the excess solid by filtration, cool down the solution to room temperature slowly and harvest the crystals by filtration; for form III, dissolve 250 mg 2-HNA and 25 mg of *p*-TsOH in 25 mL water with heating, remove the excess solid by filtration, cool down the solution to room temperature gradually and recover the crystals by filtration; for form IV, dissolve 250 mg of 2-HNA and 5 mg *p*-TsOH in 25 mL ethanol with heating, remove the excess solid by filtration, cool down the solution to room temperature gradually and harvest the crystals by filtration. The identity of the crystals was confirmed by powder X-ray diffraction and, when high quality single crystals were obtained, single crystal X-ray diffraction.

Diffraction data on 2-HNA crystals were collected at 90 K with a *Nonius* kappaCCD diffractometer.¹¹ Cell refinement and data reduction were performed with SCALEPACK and DENZO-SMN.¹² Structure solution and refinement were achieved with SHELXS97 and SHELXL97,¹³ respectively.

Thermal analyses were performed on TA Instruments Q20 (DSC), Q200 (Modulated temperature DSC or MTDSC), and INSTEC STC200 (HSM). For the DSC experiments, Tzero pans and aluminum hermetic lids were used for measuring, in general, a few milligrams of samples. The heating rate of 10 °C min⁻¹ was applied. A temperature modulation of ±0.80 °C every 60 seconds and a heating rate of 5 °C min⁻¹ were applied for MTDSC. For HSM, a few crystals were placed on a glass slide, and a programmed heating method was used. The process was captured with a digital camera. Powder X-ray diffraction (PXRD) of each sample was collected with a Rigaku X-ray diffractometer with Cu K α radiation (40 kV, 44 mA, and $\lambda = 1.5406 \text{ \AA}$) between 5.0–50.0° (2θ) at ambient temperature.

Each sample was ground and then placed on a quartz plate in an aluminum sample holder.

2.3 Computational details

2.3.1 Fukui function and dual descriptor. Fukui functions^{14–16} and dual descriptor¹⁷ within the framework of conceptual density functional theory (CDFT)^{18,19} were calculated to investigate the electron-donating and accepting abilities of atoms in 2-HNA single molecule. For Fukui functions, the condensed forms (f_k) for an atom k are usually evaluated from differences in atomic charges:

$$f_k^+ = q_k(N) - q_k(N + 1), \quad \text{governing nucleophilic attack}$$

$$f_k^- = q_k(N - 1) - q_k(N), \quad \text{governing nucleophilic attack}$$

where q_k is the partial charge of atom k and N is the number of electrons. Then the dual descriptor can be calculated as $f_k^{(2)} = f_k^+ - f_k^-$. The sign of the dual descriptor can be used to illustrate the nucleophilic or electrophilic behavior of a site within a molecule. The B3LYP^{20,21} hybrid functional with 6-311++G(d,p) basis set was employed for the geometry optimization and frequency calculation. Natural population analysis^{22,23} was also conducted at the B3LYP/6-311++G(d,p) level of theory. The corresponding total energies at 298.15 K corrected by zero point energy (ZPE) were calculated at the same level of theory.

2.3.2 Lattice energy calculations. Lattice energy of solved crystal structures was evaluated by a periodic density functional theory (DFT) method augmented by empirical potentials of long-range van der Waals.^{24,25} The periodic quantum mechanical program, Crystal 06,²⁶ was utilized for the energy calculation with B3LYP/6-21G(d,p). A crystal structure was first optimized with the lattice parameters kept constant prior to the single-point energy evaluation. BSSE (basis set superposition error) was corrected by the counterpoise method.²⁷ The energy convergence of the optimization and energy calculation was set to 10^{-7} Hartree. Root-mean-squares of energy gradient and atomic displacement were set to 0.0003 and 0.0012 atomic units, respectively.

2.3.3 Conformational search. The energies of 2-ODHPCA single molecule with different conformations were evaluated using Gaussian 09 program.²⁸ Molecules from various initial conformations were optimized at the B3LYP/6-311++G(d,p) level of theory to identify the most stable conformation, which was then used for the torsion angle scanning with all bond lengths and bond angles fixed. The same method of B3LYP/6-311++G(d,p) was used for the conformational search.

3. Results and discussion

3.1 Crystal structures

Four polymorphs were produced under different conditions. Typical crystals for the four forms are shown in Fig. 1. Table 3 lists the lattice parameters and measurement conditions of

four polymorphs of 2-HNA, or to be exact, 2-ODHPCA. They are all monoclinic with centrosymmetry. Their calculated density values are extremely close, demonstrating similar packing. The asymmetric unit of all four forms contains one molecule ($Z' = 1$) and the molecules have an almost perfectly planar conformation (Fig. 2). The torsion angles (Scheme 1) are 178.3, -177.3 , 179.8, and -178.5° for molecules in forms I–IV, respectively. Clearly, the conformational difference is insignificant. In addition, the carboxyl groups of the polymorphs show an *anti* conformation.^{29,30} Because of the *anti* conformation, the common carboxyl dimer motif is not observed in form I. Instead, as shown in Fig. 3a, one-dimensional hydrogen-bonded chains along the [001] direction are formed *via* intermolecular N–H \cdots O hydrogen bonds (N \cdots O = 2.79 Å and \angle N–H \cdots O = 164.0°), which can be graphically denoted as C(6). Intramolecular O–H \cdots O hydrogen bonded loops (O \cdots O = 2.50 Å and \angle O–H \cdots O = 154.1°), S(6) also exist. In form II, a hydrogen-bonding dimer motif between the amide functional groups that can be denoted as an intermolecular R $\frac{2}{2}$ (8) loop (N \cdots O = 2.79 Å and \angle N–H \cdots O = 168.9°) is observed as illustrated in Fig. 3b. There is also no carboxyl hydrogen-bonding dimer as in form I; instead, neighboring hydroxyl groups form hydrogen bonds (O \cdots O = 2.92 Å and \angle O–H \cdots O = 107.2°), extending the amide dimers along the [010] direction. Moreover, there is an intramolecular hydrogen bond between the hydroxyl and 2-carbonyl (O \cdots O = 2.56 Å and \angle O–H \cdots O = 152.8°), leading to an S(6) loop. Shown in Fig. 3c is the crystal packing of form III, which closely resembles the amide hydrogen-bonding dimers in form II but with slightly different hydrogen-bond lengths and angles (N \cdots O = 2.83 Å and \angle N–H \cdots O = 162.1°). Also observed is the intramolecular hydrogen bond (O \cdots O = 2.55 Å and \angle O–H \cdots O = 153.0°), but because of a larger

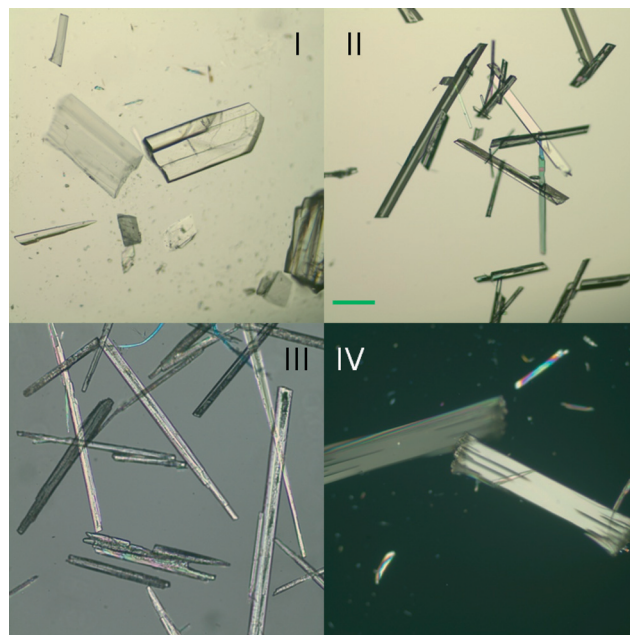
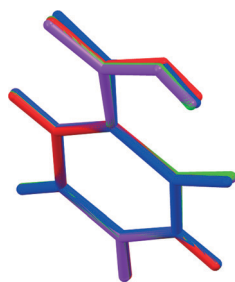


Fig. 1 Crystals of the four polymorphs of 2-ODHPCA. Scale bar: 0.2 mm.

Table 3 Crystallographic data of four forms of 2-ODHPCA

Form	I	II	III	IV
Formula	C ₆ H ₅ NO ₃	C ₆ H ₅ NO ₃	C ₆ H ₅ NO ₃	C ₆ H ₅ NO ₃
Formula weight	139.11	139.11	139.11	139.11
Crystal size (mm ³)	0.30 × 0.20 × 0.15	0.40 × 0.10 × 0.10	0.30 × 0.20 × 0.20	0.50 × 0.18 × 0.05
Crystal system	Monoclinic	Monoclinic	Monoclinic	Monoclinic
Space group	<i>P</i> 2 ₁ / <i>n</i>	<i>P</i> 2 ₁ / <i>n</i>	<i>P</i> 2 ₁ / <i>c</i>	<i>P</i> 2 ₁ / <i>c</i>
<i>a</i> /Å	3.640(1)	3.725(1)	9.997(2)	9.773(2)
<i>b</i> /Å	11.584(3)	7.368(2)	3.754(1)	4.0520(8)
<i>c</i> /Å	13.565(3)	20.417(4)	15.362(3)	14.993(5)
α /°	90	90	90	90
β /°	94.64(1)	91.47(4)	106.31(3)	109.95(5)
γ /°	90	90	90	90
<i>Z</i> , <i>Z'</i>	4, 1	4, 1	4, 1	4, 1
<i>V</i> /Å ³	570.1(2)	560.2 (2)	553.3(2)	558.1(2)
<i>D</i> _{cal} /g cm ⁻³	1.621	1.649	1.670	1.656
<i>T</i> /K	90 (2)	90 (2)	90(2)	90(2)
Abs coeff (mm ⁻¹)	0.133	0.135	0.137	0.136
<i>F</i> (000)	288.0	288.0	288.0	288.0
θ range(deg)	2.32–27.47	2.00–27.50	2.12–27.49	2.22–27.52
Limiting indices	-4 ≤ <i>h</i> ≤ 4 -15 ≤ <i>k</i> ≤ 15 -17 ≤ <i>l</i> ≤ 17	-4 ≤ <i>h</i> ≤ 4 -9 ≤ <i>k</i> ≤ 9 -26 ≤ <i>l</i> ≤ 26	-12 ≤ <i>h</i> ≤ 12 -4 ≤ <i>k</i> ≤ 4 -19 ≤ <i>l</i> ≤ 19	-12 ≤ <i>h</i> ≤ 12 -5 ≤ <i>k</i> ≤ 5 -19 ≤ <i>l</i> ≤ 19
Completeness to 2 θ	100.0%	100.0%	100%	100%
Unique reflections	1307	1292	1263	1277
<i>R</i> ₁ [<i>I</i> > 2 σ (<i>I</i>)]	0.0451	0.0457	0.0427	0.0379
w <i>R</i> ₂ (all data)	0.1300	0.1274	0.1187	0.1165

**Fig. 2** Superposition of four molecules from the asymmetric units of the four polymorphs (I, blue; II, red; III, green; and IV, purple).

distance between neighboring hydroxyl groups ($O\cdots O = 3.20 \text{ \AA}$), there is no hydrogen bonding that ties the amide dimers as in form II. More interestingly, the almost identical packing patterns and hydrogen-bonding motifs are present in form IV except for the intermolecular hydrogen bonding distance and angle are different ($N\cdots O = 2.80 \text{ \AA}$ and $\angle N-H\cdots O = 174.0^\circ$), as shown in Fig. 3d. The intramolecular hydrogen bond has similar parameters to that of form III ($O-O = 2.57 \text{ \AA}$ and $\angle O-H\cdots O = 152.9^\circ$). The lattice parameters between the two forms are also very close (Table 2). Crystal structures that were solved at room temperature also indicate that they are two distinct polymorphs and each form is thermally stable (from 90 K to room temperature), except for slight axes elongation and the beta angle increase. The structural difference is also supported by the PXRD and DSC results, as discussed below.

3.2 Thermal properties

DSC with hermetically sealed pans was conducted to investigate relative stability and possible phase transitions of the

four polymorphs. The thermograms are shown in Fig. 4. Form I demonstrates one single thermal event with the onset temperature of 261.4 °C; the endothermic peak is the melting of the crystal. Two endothermic peaks of form II are observed. The first peak with the onset temperature of 253.3 °C is due to a solid–solid phase transition to another form. The solid–solid phase transition was verified by melting a single crystal of form II in a sealed capillary tube on the hot stage (Fig. 5) as well as modulated temperature DSC (Fig. 6a). The MTDSC indicated that the phase transition was irreversible crystallization. The second peak with the onset temperature 261.6 °C coincides with the melting of form I, suggesting that the new form is form I. On cursory examination, form III only shows one endothermic peak which is almost identical to that of form I. But in reality, Form III undergoes a solid–solid phase transition to form II at around 160 °C. This phase transition was also confirmed by hot-stage microscopy study (not shown), PXRD results (Fig. 7), and MTDSC experiment (Fig. 6b). Similar to form II, the MTDSC suggested the phase transition was irreversible crystallization. Form IV seems to have the same DSC trace as form II. But in actuality, form IV also experiences a phase transition to form II at around 155 °C. The phase transition was also verified by HSM, PXRD, and MTDSC (Fig. 6c). When all of the DSC samples were cooled to ambient temperature after the melting, one exothermal peak was observed around 235 °C (not shown), indicating recrystallization of the melt. The crystals from recrystallization were characterized by PXRD to be form I.

Crystal samples were observed under a hot-stage microscope. It was found that, when heated on the hot stage,

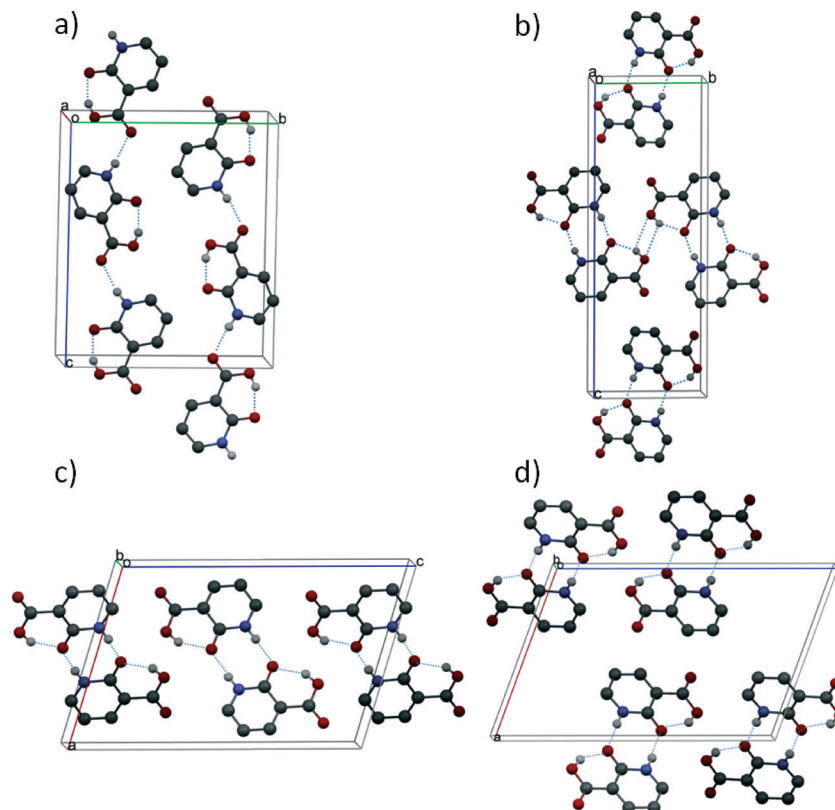


Fig. 3 Crystal packing of forms I (a), II (b), III (c), and IV (d).

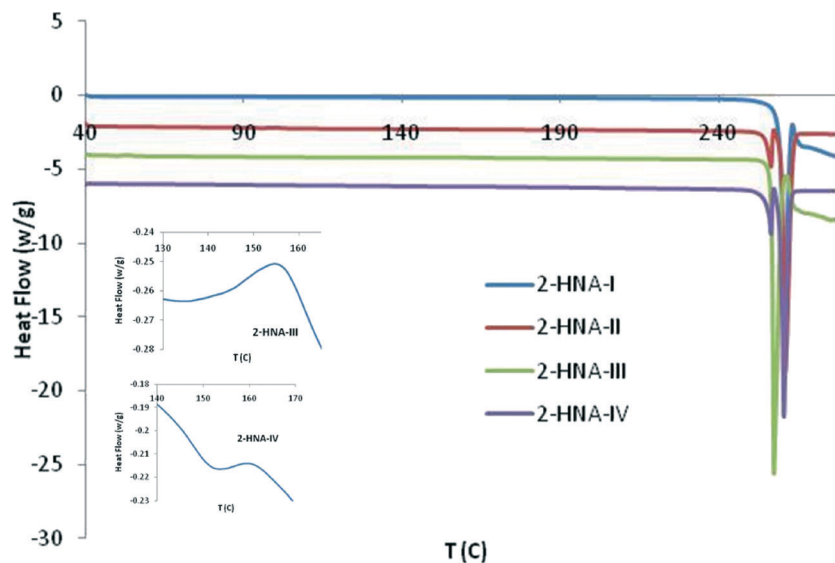


Fig. 4 DSC thermograms of the four polymorphs (the insets are phase transitions for forms III and IV, respectively).

crystals of four forms started to sublime respectively at about 175 °C (at that temperature, forms III and IV should have already converted into form II). The vapor then condensed onto the cover glass slip of the hot stage. The crystals formed by sublimation were confirmed by single crystal X-ray diffraction to be form I regardless which polymorph to start with.

3.3 pH effect

From the crude product, three forms (I, II, and III) were obtained from ethyl acetate, water and methanol, correspondingly. The crystallization results seemed to suggest that solvent alone may have played a role in the polymorphs formation. Surprisingly, all the crystal growth trials with just commercial

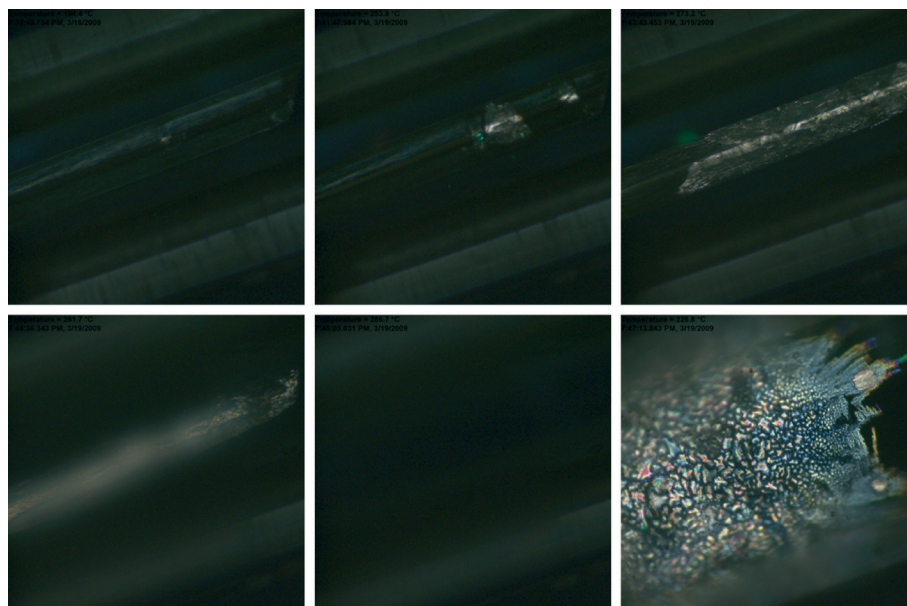


Fig. 5 Solid-solid phase transition from form II to I, melting of form I, and recrystallization of form I.

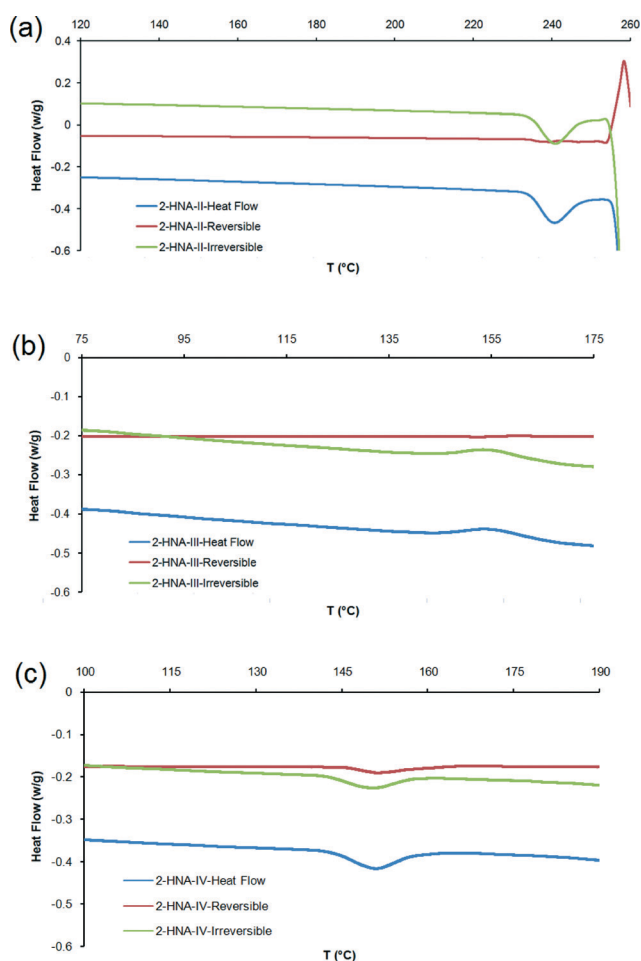


Fig. 6 Modulated temperature DSC results of forms II (a), III (b) and IV (c).

2-HNA yielded only form II when attempts were made to scale up the three forms for further study and to attain a real crystal

of 2-HNA (Table 1). Disappearing polymorphism was thought to be the explanation for this system.³¹ But additives were considered as a possible cause for the other two polymorphs as well. Investigation of the purity of the crude product with NMR disclosed starting materials including *p*-TsOH, other than 2-HNA. Likely, one or some combinations of the reactants induced the formation of the other two forms. Control experiments showed that in the presence of only 2-CNA, all solutions led to form II; with the addition of DCMA, again only form II was produced; but when *p*-TsOH was introduced, the MeOH solution produced form I, and some of the EtOH solutions gave form IV (Table 2). *p*-TsOH is a strong organic acid and it might change the pH of the solutions and thus lead to the formation of the other two forms. Replacing *p*-TsOH with a mineral acid, HCl, a similar effect was achieved: in MeOH, form I was harvested, and in other solutions, only form II was reaped. Another mineral acid, H₂SO₄, affected the crystallization of 2-HNA the same way as did HCl.

2-HNA is similar to an acidic amino acid. In fact, it is a vinylogous amino acid. It dissociates in aqueous or even

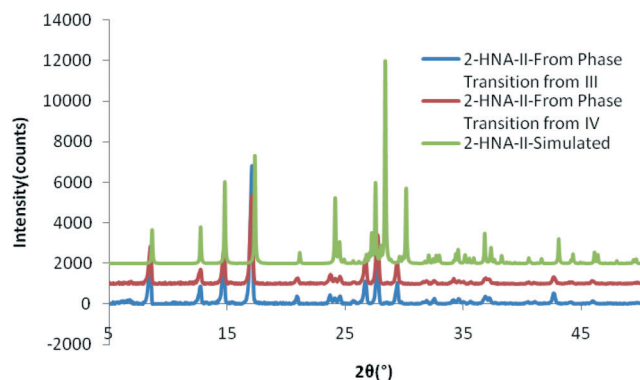


Fig. 7 PXRD of forms III and IV after the phase transition.

organic solvents. The presence of other acids in the same system (*i.e.*, pH change) should affect the proton dissociation and thus the crystal formation of 2-HNA, perhaps comparable to the well-studied pH effect on the polymorphism of glycine.^{32–34} Stephens *et al.* investigated 2-HNA over a wide range of pH with UV-Vis spectrophotometry.³⁵ According to their study, with pH less than 0, the compound exists as a protonated state, with pH between 0 and 5, it takes the zwitterion form with the N protonated, when the pH is between 5 and 12, the carboxylic acid is deprotonated, while pH higher than 12, both acidic protons are removed. Thus, in a subtle way, the combination of acid and solvent played a role in the production of the polymorphs for 2-HNA. To eliminate the complexity introduced by acid dissociation in organic solvents, experiments were carried out in water with or without adjusting the pH. All four forms were obtained, sometimes as pure forms, other times as mixtures. Attempts were made to establish a direct relationship between a peculiar pH and a specific form, but success was limited. Moreover, Fig. 8 shows experimental powder X-ray diffraction patterns of crystal samples together with simulated patterns based on the single crystal structures. The close matching of diffraction patterns indicate that samples of forms I, II, III, and IV were polymorphically pure.

3.4 Quantum chemical calculations

Density functional theory (DFT) study provided important evidence that 2-ODHPCA is the predominant form of 2-HNA in the gas phase. In the current study, eight isomers of neutral

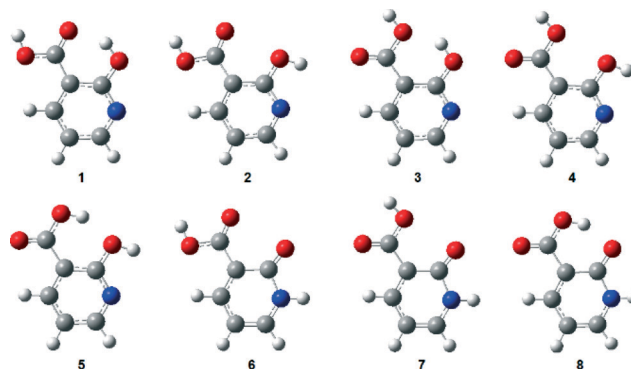


Fig. 9 Eight isomers of 2-HNA.

2-HNA including five enol forms and three keto forms were investigated, and their optimized structures are depicted in Fig. 9. The total energies E , zero-point energies E_{ZPE} , relative energies ΔE , Boltzmann distribution and intramolecular interaction energy ΔE_{intra} are summarized in Table 4. Herein, the relative energies ΔE and the Boltzmann distribution are calculated by the following equations:

$$\Delta E = E_i - E_0$$

$$N_i = N_0 \exp\left(\frac{-\Delta E_i}{RT}\right)$$

where N_0 is the total number of particles at the lowest energy level, N_i is the number of particles at the energy level i ,

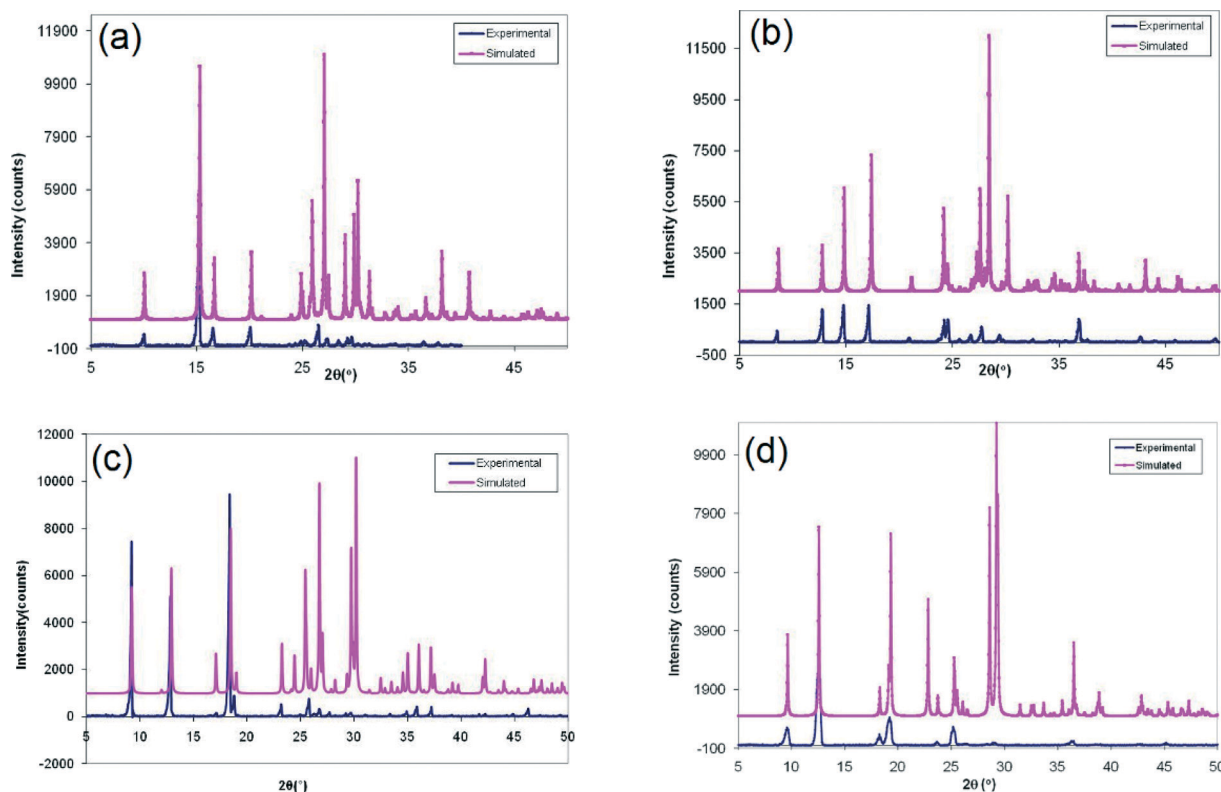


Fig. 8 Experimental and simulated powder X-ray diffraction patterns of 2-ODHPCA polymorphs, form I (a), II (b), III (c), and IV (d).

Table 4 Total energies E (in Hartree), zero-point energies E_{ZPE} (in Hartree), relative energies ΔE (in kJ mol^{-1}), Boltzmann distribution and intramolecular interaction energy ΔE_{intra} (in kJ mol^{-1}) of eight isomers

Isomer	E	E_{ZPE}	ΔE	Boltzmann distribution/%	$\Delta E_{\text{intra}}^a$
1	-512.25031	0.10827	12.35	0.68624	-19.26
2	-512.24265	0.10794	31.61	0.00029	—
3	-512.24504	0.10787	25.14	0.00394	-4.18
4	-512.24354	0.10796	29.32	0.00073	—
5	-512.24486	0.10769	25.14	0.00394	-4.18
6	-512.24295	0.10788	30.66	0.00043	—
7	-512.24499	0.10815	25.99	0.00283	—
8	-512.25534	0.10860	0.00	99.30160	-25.99

^a ΔE_{intra} value is the energy difference between isomers 1 and 2, 3 and 4, 5 and 4, 8 and 7, respectively.

E_i is the total energy per mole molecule occupying state i , E_0 is the total energy per mole molecule at the lowest energy level, ΔE is their difference, R is universal gas constant ($8.314 \times 10^{-3} \text{ kJ mol}^{-1} \text{ K}^{-1}$), T is 298.15 K.

It is evident that isomer 8 (2-ODHPCA) is the most stable, and the Boltzmann distribution indicates that isomer 8 predominates over the other isomers, being almost the only form in the gas phase (99.30%). This result is in good agreement with that of Dogra.⁸ Remarkably, isomer 8 has the strongest intramolecular hydrogen-bonding interaction, which accounts for its stability.

The Fukui function and the dual descriptors are used to characterize the site-specific reactivity or local preference of molecular interactions of atoms in 2-ODHPCA, summarized in Table 5. The atoms are numbered in Fig. 10a. It can be seen that the negative values of dual descriptors suggest that atoms O10, O8, O9 and N1 are considerably nucleophilic, and this is also confirmed by the large values of their condensed Fukui functions f^- (nucleophilic). In the meantime, they bear highly negative atomic charges, indicating their nucleophilic characteristics.

DSC and hot-stage results suggest that form I is the most stable polymorph at room and higher temperatures. Lattice energies calculated with the empirically augmented DFT method are -115.372 , -118.882 , -115.997 , and $-118.490 \text{ kJ mol}^{-1}$ of forms I-IV, respectively. The calculation results are very close, roughly within 3 kJ mol^{-1} , and the difference between forms I and III or II and IV is almost negligible. The calculation indicates that form II, not form I, is the most stable form. Note that the calculations were implicitly conducted at zero Kelvin and no entropic input was considered.

Table 5 Condensed atomic charge (q), electrophilic (f^+) and nucleophilic (f^-) Fukui functions, dual descriptors ($f_k^{(2)}$) of selected atoms

Atom	q	f^+	f^-	$f_k^{(2)}$
O10	-0.667	-0.296	0.275	-0.571
O8	-0.673	-0.293	0.371	-0.664
O9	-0.592	-0.227	0.281	-0.508
N1	-0.541	-0.175	0.259	-0.434

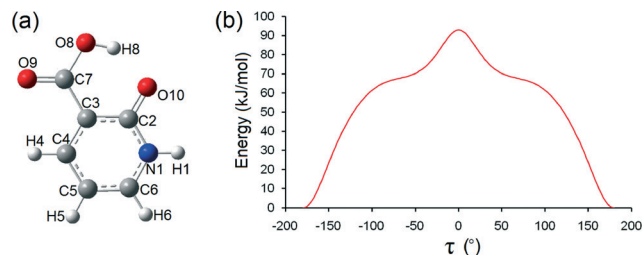


Fig. 10 (a) 2-ODHPCA single molecule; (b) conformational energy as a function of torsion angle τ relative to the lowest-energy conformer.

The discrepancy of the thermal stability order between the experimental observation and lattice energy calculation may be due to the temperature effect and the relative stability order may switch over a wide range of temperature. Nevertheless, based on the empirical rules proposed by Burger and Ramberger,³⁶ form I is enantiotropically related to the other three forms since it has the lowest density yet the highest melting point (density rule). The enantiotropism between forms I and II is also possible since an endothermic phase transition was observed (heat-of-transition rule). Forms III and II, as well as form IV and II, are monotropically related since the phase transitions are exothermic (heat-of-transition rule). Form III is more stable than form IV at zero Kelvin at least based on the densities.

In all four polymorphs, the C-C bond between -COOH and the aromatic ring of the molecule is mainly single suggested by the bond length of 1.49 \AA . It is very likely that the -COOH is no longer in tight conjugation with the aromatic ring and thereby rotation about the C-C bond is feasible to some extent. As such, despite nearly identical conformations of molecules in the polymorphs (Fig. 2), energy calculations of other conformations were conducted as a function of the torsion angle τ . As illustrated in Fig. 10b, the global minimum is at $\pm 180^\circ$ and no local minima exist. This is in agreement with the experimental values of the torsion angles and molecular conformations and can be explained by the rigidity caused by the intramolecular S(6) hydrogen bond. It may be then argued that the polymorphism of 2-HNA or, to be accurate, 2-ODHPCA, stems from the spatial tessellation that is directed by intermolecular hydrogen bonding.

3.5 Hirshfeld surface analyses

To further understand relative contributions to intermolecular interactions by various molecular contacts in the polymorphs, Hirshfeld surface analyses^{37,38} were performed with CrystalExplorer (Version 3.1),³⁹ and the results are shown in Fig. 11. It is evident that hydrogen-bonded contacts contribute to nearly 60% of the Hirshfeld surface in any of four forms and the O...H contacts predominate over other interactions. C...H contacts also play a significant role (>10%). The contribution by C...O contacts ranges from 5% to 9%, normally associated with $n-\pi$ interactions between the

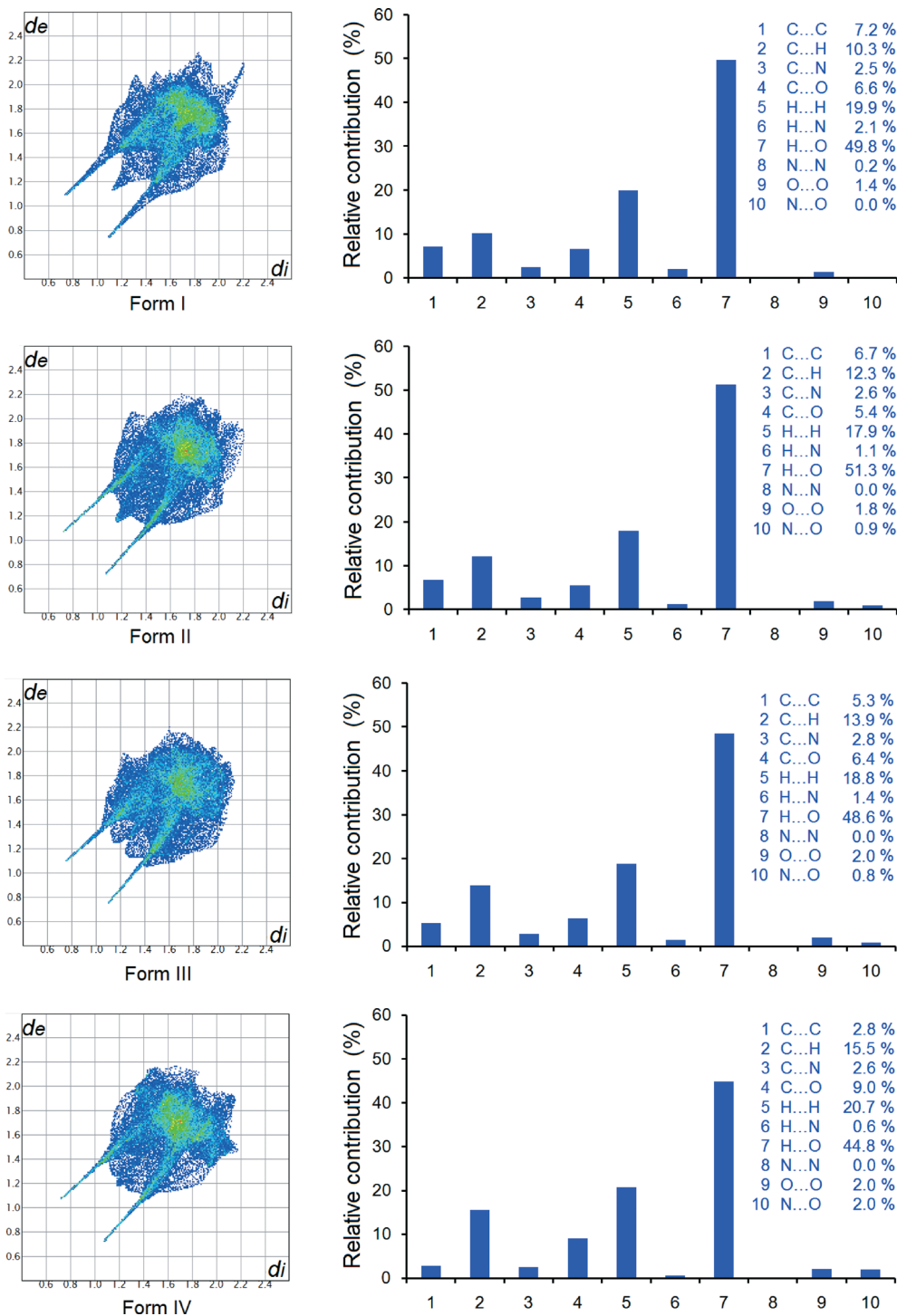


Fig. 11 2D fingerprint plots (left) for four forms (I, II, III and IV) and relative contributions to the Hirshfeld surface (right) by the various intermolecular contacts in the four forms.

lone pair orbitals of the O atom and the π orbitals of the C=C double bond. C...C contacts possibly due to π - π interactions between aromatic rings can be seen in all of the four forms, but less significant in form IV than in form I, II, or III. The analyses thus support the notion that crystal structures are maintained mainly by hydrogen bonding and facilitated by π - π interactions.

4. Conclusions

Despite being marketed as 2-HNA, the real identity of solid samples of the compound was revealed to be the tautomer 2-ODHPCA and four polymorphs were discovered serendipitously. The polymorphism is due to the packing arrangements in the crystals since the molecules in the unit cells are

essentially identical. The results of a series of crystal growth experiments suggest that pH and solvent play important roles in the formation of these polymorphs. The possible hydrogen-bonding sites in the crystals can be well predicted by analyzing the site-specific reactivity of atoms in 2-ODHPCA via the condensed Fukui function and the dual descriptor. Lattice energy calculations by DFT and thermal study by DSC provided clues to the relative stability of four forms. HSM revealed solid–solid phase transitions from form II to I, forms III and IV to II. Conformational search did not suggest possible conformational polymorphs. Meanwhile, similar compounds such as 4-hydroxynicotinic acid and 6-hydroxynicotinic acid also exist in the ketonic form in the solid state,⁴⁰ yet no crystal structure of 5-hydroxynicotinic acid is reported. And neither 4-hydroxynicotinic acid nor 6-hydroxynicotinic acid is polymorphic although 4-hydroxynicotinic acid does have a hemihydrate form reported.⁴¹ Whether it is due to a lack of effort of polymorph screening or unique molecular properties remains to be explored.

Acknowledgements

SL thanks Natural Science Foundation of Hubei Province for financial support (2014CFB787). PZ thanks the financial support by the National Natural Science Foundation of China (grant no. 21403097) and the Fundamental Research Funds for the Central Universities (Izujbky-2014-182). TL thanks NSF for financial support (DMR-1006364). The authors are also grateful to Dr. Sean Parkin for providing laboratory facilities and helpful discussion.

References

- O. N. Miller, *Ger. Pat.*, DE 2157333, 1972.
- A. Tinschert, A. Kiener, K. Heinzmann and A. Tscherch, *Arch. Microbiol.*, 1997, **168**, 355–361.
- R. Weyer, V. Hitzel and E. Granzer, *Ger. Pat.*, DE 2637477, 1978.
- S. M. O. Quintal, H. I. S. Nogueira, V. Felix and M. G. B. Drew, *Polyhedron*, 2002, **21**, 2783–2791.
- Y.-F. Yue, W. Sun, E.-Q. Gao, C.-J. Fang, S. Xu and C.-H. Yan, *Inorg. Chim. Acta*, 2007, **360**, 1466–1473.
- A. Boulton and A. McKillop, *Comprehensive Heterocyclic Chemistry: the Structure, Reactions, Synthesis and Uses of Heterocyclic Compounds*, Pergamon, Oxford, 1984.
- M. S. Saleh, K. A. Idriss, M. S. Abu-Bakr and E. Y. Hashem, *Analyst*, 1992, **117**, 1003–1007.
- S. K. Dogra, *J. Mol. Struct.*, 2005, **737**, 189–199.
- S. Long, M. Siegler and T. Li, *Acta Crystallogr., Sect. E: Struct. Rep. Online*, 2006, **62**, O5664–O5665.
- R. C. Santos, R. M. B. B. M. Figueira, M. F. M. Piedade, H. P. Diogo and M. E. M. da Piedade, *J. Phys. Chem. B*, 2009, **14291**–14309.
- Nonius, Collect, Nonius BV, Delft, the Netherlands*, 2002.
- Z. Otwinowski and W. Minor, in *Methods in Enzymology: Macromolecular Crystallography, Part A*, ed. C. W. Carter Jr. and R. M. Sweet, Academic Press, New York, 1997, vol. 276, pp. 307–326.
- G. M. Sheldrick, *SHELXL97 and SHELXS97*, University of Gottingen, 1997.
- P. W. Ayers and M. Levy, *Theor. Chem. Acc.*, 2000, **103**, 353–360.
- R. G. Parr and W. Yang, *J. Am. Chem. Soc.*, 1984, **106**, 4049–4050.
- W. Yang and R. G. Parr, *Proc. Natl. Acad. Sci. U. S. A.*, 1985, **82**, 6723–6726.
- C. Morell, A. Grand and A. Toro-Labbe, *J. Phys. Chem. A*, 2005, **109**, 205–212.
- P. Geerlings, F. D. Proft and W. Langenaeker, *Chem. Rev.*, 2003, **103**, 1793–1874.
- S. B. Liu, *Wuli Huaxue Xuebao*, 2009, **25**, 590–600.
- A. D. Becke, *J. Chem. Phys.*, 1993, **98**, 5648–5652.
- C. Lee, W. Yang and R. G. Parr, *Phys. Rev. B: Condens. Matter Mater. Phys.*, 1988, **37**, 785–789.
- A. E. Reed, L. A. Curtiss and F. Weinhold, *Chem. Rev.*, 1988, **88**, 899–926.
- J. P. Foster and F. Weinhold, *J. Am. Chem. Soc.*, 1980, **102**, 7211–7218.
- T. Li and S. Feng, *Pharm. Res.*, 2006, **23**, 2326–2332.
- S. Feng and T. Li, *J. Chem. Theory Comput.*, 2006, **2**, 149–156.
- R. Dovesi, R. Orlando, B. Civalleri, C. Roetti, V. R. Saunders and C. M. Zicovich-Wilson, *Z. Kristallogr.*, 2005, **220**, 571–573.
- S. F. Boys and F. Bernardi, *Mol. Phys.*, 1970, **19**, 553–566.
- M. J. Frisch, G. W. Trucks, H. B. Schlegel, G. E. Scuseria, M. A. Robb, J. R. Cheeseman, G. Scalmani, V. Barone, B. Mennucci, G. A. Petersson, H. Nakatsuji, M. Caricato, X. Li, H. P. Hratchian, A. F. Izmaylov, J. Bloino, G. Zheng, J. L. Sonnenberg, M. Hada, M. Ehara, K. Toyota, R. Fukuda, J. Hasegawa, M. Ishida, T. Nakajima, Y. Honda, O. Kitao, H. Nakai, T. Vreven, J. A. Montgomery Jr., J. E. Peralta, F. Ogliaro, M. Bearpark, J. J. Heyd, E. Brothers, K. N. Kudin, V. N. Staroverov, R. Kobayashi, J. Normand, K. Raghavachari, A. Rendell, J. C. Burant, S. S. Iyengar, J. Tomasi, M. Cossi, N. Rega, N. J. Millam, M. Klene, J. E. Knox, J. B. Cross, V. Bakken, C. Adamo, J. Jaramillo, R. Gomperts, R. E. Stratmann, O. Yazyev, A. J. Austin, R. Cammi, C. Pomelli, J. W. Ochterski, R. L. Martin, K. Morokuma, V. G. Zakrzewski, G. A. Voth, P. Salvador, J. J. Dannenberg, S. Dapprich, A. D. Daniels, O. Farkas, J. B. Foresman, J. V. Ortiz, J. Cioslowski and D. J. Fox, *Gaussian 09, Revision, A. 02*, Gaussian, Inc., Wallingford CT, 2009.
- M. Fujinaga and M. N. G. James, *Acta Crystallogr., Sect. B: Struct. Crystallogr. Cryst. Chem.*, 1980, **36**, 3196–3199.
- L. Leiserowitz, *Acta Crystallogr., Sect. B: Struct. Crystallogr. Cryst. Chem.*, 1976, **32**, 775–802.
- J. Dunitz and J. Bernstein, *Acc. Chem. Res.*, 1995, **28**, 193–200.
- I. S. Lee, K. T. Kim, A. Y. Lee and A. S. Myerson, *Cryst. Growth Des.*, 2008, **8**, 108–113.
- C. S. Towler, R. J. Davey, R. W. Lancaster and C. J. Price, *J. Am. Chem. Soc.*, 2004, **126**, 13347–13353.
- L. Yu and K. Ng, *J. Pharm. Sci.*, 2002, **91**, 2367–2375.

- 35 A. K. W. Stephens and C. Orvig, *Inorg. Chim. Acta*, 1998, 273, 47–53.
- 36 A. Burger and R. Ramberger, *Microchim. Acta*, 1979, 2, 259–271.
- 37 F. L. Hirshfeld, *Theor. Chim. Acta*, 1977, 44, 129–138.
- 38 M. A. Spackman and D. Jayatilaka, *CrystEngComm*, 2009, 11, 19–32.
- 39 S. K. Wolff, D. J. Grimwood, J. J. McKinnon, M. J. Turner, D. Jayatilaka and M. A. Spackman, *University of Western Australia*, 2012.
- 40 S. Gupta, S. Long and T. Li, *Acta Crystallogr., Sect. E: Struct. Rep. Online*, 2007, 63, o2784.
- 41 E. P. Matias, C. E. S. Bernardes, M. F. M. Piedade and M. E. Minas da Piedade, *Cryst. Growth Des.*, 2011, 11, 2803–2810.